

Gene Regulation by Riboswitches with and without Negative Feedback Loop

Jong-Chin Lin* and D. Thirumalai*

Department of Chemistry and Biochemistry, Biophysics Program, Institute for Physical Science and Technology, University of Maryland, College Park, Maryland

ABSTRACT Riboswitches, structured elements in the untranslated regions of messenger RNAs, regulate gene expression by binding specific metabolites. We introduce a kinetic network model that describes the functions of riboswitches at the systems level. Using experimental data for flavin mononucleotide riboswitch as a guide, we show that efficient function, implying a large dynamic range without compromising the requirement to suppress transcription, is determined by a balance between the transcription speed, the folding and unfolding rates of the aptamer, and the binding rates of the metabolite. We also investigated the effect of negative feedback accounting for binding to metabolites, which are themselves the products of genes that are being regulated. For a range of transcription rates negative feedback suppresses gene expression by nearly 10-fold. Negative feedback speeds the gene expression response time, and suppresses the change of steady-state protein concentration by half relative to that without feedback, when there is a modest spike in DNA concentration. A dynamic phase diagram expressed in terms of transcription speed, folding rates, and metabolite binding rates predicts different scenarios in riboswitch-mediated transcription regulation.

INTRODUCTION

Riboswitches are *cis*-acting RNA elements located in the untranslated region of mRNAs that regulate associated gene expression by sensing and binding target cellular metabolites (1–3). In bacteria, binding of metabolites to the conserved aptamer domain allosterically alters the folding patterns of the downstream expression platform, whose conformation controls transcription termination or translation initiation (2,4,5). The target metabolites are usually the products or their derivatives of the downstream gene that riboswitches control. Hence, metabolite binding to riboswitches serves as a feedback signal to control RNA transcription or translation initiation. The feedback through metabolite binding is naturally designed to be a fundamental network motif for riboswitches. For example, tandem riboswitches respond to multiple metabolites to control a single gene with greater regulatory complexity (6,7), whereas single glmS riboswitch has been shown to respond to multiple signals using both negative and positive feedback (8). Understanding the various *in vivo* riboswitch functions requires a theoretical framework that takes into account the interplay between speed of RNA transcription, folding kinetics of the nascent RNA transcript, and kinetics of metabolite binding to the nascent RNA transcript, and the role of feedback arising from interactions between synthesized metabolites and the transcript. The effects of speed of RNA transcription and metabolite binding kinetics have been examined *in vitro* in an insightful study involving the flavin mononucleotide (FMN) riboswitches (9). They argued that FMN riboswitch is kinetically driven implying

that the riboswitch does not reach thermodynamic equilibrium with FMN before a decision between continued transcription and transcription termination needs to be made.

The regulatory roles played by riboswitches have also inspired the design of novel RNA-based gene-control elements that respond to small molecules (10,11). Several models have been proposed to describe how riboswitches function and meet their regulatory demands (12,13). However, they focused solely on the transcription process without accounting for the feedback effect from the metabolite produced by the gene encoding the riboswitch. Here, we introduce a general kinetic network model that can be used to describe both *in vivo* and *in vitro* functions of riboswitches. Our coarse-grained kinetic network model, which takes into account the interplay of cotranscriptional folding, speed of transcription, and kinetics of metabolite binding, also models effects of a negative feedback loop so that predictions for *in vivo* functions of riboswitches can be made. As an illustration of the theory, we first consider the dependence of metabolite concentration on the regulation of *in vitro* transcription termination of FMN riboswitches without a feedback loop, which enables us to obtain the range of folding rates and transcription rates that produce results consistent with experiments (9). We then include the negative feedback loop in the network to study how riboswitches regulate gene expression at the systems level.

METHODS

General kinetic model

The riboswitch is transcribed from the leader, the nonprotein-coding region, of the associated gene (Fig. 1). We simplify the multiple complex *in vitro* biochemical steps in the function of the off riboswitch, involving

Submitted June 3, 2012, and accepted for publication October 23, 2012.

*Correspondence: thirum@umd.edu or jclin@umd.edu

Editor: Samuel Butcher.

© 2012 by the Biophysical Society
0006-3495/12/12/2320/11 \$2.00

<http://dx.doi.org/10.1016/j.bpj.2012.10.026>

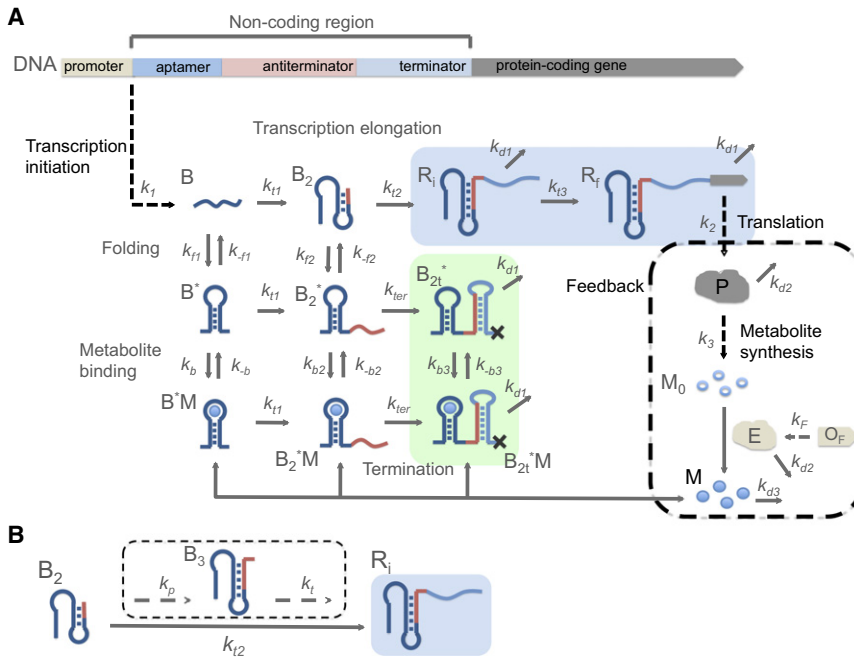


FIGURE 1 (A) Kinetic network model for RNA transcription mediated by riboswitches. The leader, upstream of the protein-coding gene, consists of sequences that can be transcribed to the aptamer domain (B), antiterminator (B_2) and terminator region (R_i) of the riboswitch. After transcription initiation, elongation, folding of RNA transcript, and metabolite binding are simplified to several key steps. Starting from the transcript B , where the aptamer sequence is transcribed, transcription can continue to B_2 (antiterminator sequence transcribed) at a transcription rate constant k_{t1} . Further elongation through the terminator sequence with transcription rate constant k_{t2} results in the synthesis of full RNA without termination. R_i is the transcript with the sequence of the protein-coding region starting to be transcribed, and eventually grows to R_f , the full protein-coding region transcribed, with a rate of k_{t3} . Besides transcription elongation, each of the transcript states, B and B_2 , can form states with aptamer domain folded (B^* and B_2^*) with a folding rate of k_{f1} and k_{f2} , respectively. The aptamer folded states can bind metabolite (M) leading to the bound states (B^*M and B_2^*M) with association rate constant k_b . The transcripts in state B_2^* and B_2^*M can continue elongating until the terminator sequence is transcribed with their transcription terminating transcription, with a rate of k_{ter} (B_{2t}^* and B_{2t}^*M). The fraction of transcription termination, f_{ter} , is determined from the amount of the terminated transcripts (in green block) versus nonterminated transcripts (in blue block). In the presence of a negative feedback loop (steps included by the box in dashes) additional biochemical steps have to be included. In this case after RNA is fully synthesized, it can produce protein P at a rate k_2 or get degraded with a rate k_{d1} . The fate of P is either degradation (rate k_{d2}) or production of an inactive metabolite M_0 , which is activated by the enzyme (E) encoded by the gene O_F . The activated enzyme can bind to the folded aptamer and can abort transcription. (B) Simplification of the step from B_2 to R_i for FMN riboswitch. In the application to FMN riboswitch, B_2 represents the transcript out of the RNA polymerase at the second pause site (9). The step $B_2 \rightarrow R_i$ is a simplification of the potential multiple chemical process, including pausing and emerging of the antiterminator sequence ($B_2 \rightarrow B_3$), and transcription to the terminator sequence ($B_3 \rightarrow R_i$). The rate k_{t2} is approximated as the pausing rate k_p , because pausing is likely to be the rate-limiting step in the transcription process.

expression platform forming a transcription terminator stem and dissociate from the DNA template terminating transcription, with a rate of k_{ter} (B_{2t}^* and B_{2t}^*M). The fraction of transcription termination, f_{ter} , is determined from the amount of the terminated transcripts (in green block) versus nonterminated transcripts (in blue block). In the presence of a negative feedback loop (steps included by the box in dashes) additional biochemical steps have to be included. In this case after RNA is fully synthesized, it can produce protein P at a rate k_2 or get degraded with a rate k_{d1} . The fate of P is either degradation (rate k_{d2}) or production of an inactive metabolite M_0 , which is activated by the enzyme (E) encoded by the gene O_F . The activated enzyme can bind to the folded aptamer and can abort transcription. (B) Simplification of the step from B_2 to R_i for FMN riboswitch. In the application to FMN riboswitch, B_2 represents the transcript out of the RNA polymerase at the second pause site (9). The step $B_2 \rightarrow R_i$ is a simplification of the potential multiple chemical process, including pausing and emerging of the antiterminator sequence ($B_2 \rightarrow B_3$), and transcription to the terminator sequence ($B_3 \rightarrow R_i$). The rate k_{t2} is approximated as the pausing rate k_p , because pausing is likely to be the rate-limiting step in the transcription process.

transcription, cotranscriptional RNA folding, and metabolite binding, to a few key kinetic steps (Fig. 1). Without feedback, the first stage is the transcription of the aptamer domain (B). The antiterminator sequence is transcribed (B_2) in the second step. At each stage, the aptamer domain of the RNA transcript can either cotranscriptionally fold or unfold. Only when the aptamer domain is folded (B^* , B_2^*) can the RNA transcript bind the metabolite (M). At the second stage, when the aptamer domain is unfolded, the RNA transcript is in an alternative folding pattern with the formation of the antiterminator stem (B_2). The final stage of the transcription occurs when the terminator sequence is transcribed (R_i). If the terminator sequence is transcribed following B_2 , the antiterminator structure prevents the formation of a terminator stem and the transcription proceeds until the downstream coding region is fully transcribed (R_f). If the terminator sequence is transcribed following B_2^* or B_2^*M , the absence of antiterminator allows the terminator to form, which subsequently leads to the dissociation of RNA transcript (B_{2t}^* and B_{2t}^*M) from the DNA template and terminates the transcription. The feedback effect involved with translation and metabolite synthesis will be discussed in later sections.

To assess how the metabolite concentration, $[M]$, regulates transcription termination, we computed the fraction of terminated transcript, f_{ter} , given an initial concentration of RNA transcript with aptamer sequence transcribed (B). Some of the rate constants can be estimated from the in vitro experiments (9) for FMN riboswitches, which we use to illustrate the efficacy of the theory. The experimental values of the FMN association rate constant k_b for the FMN aptamer is $\sim 0.1 \mu M^{-1} s^{-1}$, and the dissociation rate constant k_{-b} is $\sim 10^{-3} s^{-1}$, giving the equilibrium $K_D \equiv k_{-b} / k_b = 10$ nM. RNA polymerases (RNAP) pause at certain transcription sites during transcription. There are two pause sites for the FMN riboswitch, one after

the aptamer domain sequence with a lifetime of the paused complex being ~ 10 s, and the other at the end of the antiterminator sequence with a lifetime ~ 1 min. To approximately account for the pause times in our simplified model, we observe that B_2 represents the transcript of the FMN riboswitch with part of the antiterminator out of RNAP, when RNAP pauses at the second pause site. Even with only part of the antiterminator sequence, the transcript still has high probability of forming alternate folding patterns (9), similar to a full antiterminator sequence. Hence, we set the effective transcription rates $k_{t1} = 0.1 s^{-1}$ and $k_{t2} = 0.016 s^{-1}$, which reflects the pause times for the FMN riboswitch (see Fig. 1 B for additional explanation of this approximation).

Extraction of minimal set of parameters from in vitro transcription experiments

To make testable predictions using our model, we need estimates of the cotranscriptional folding and unfolding rates of the aptamer B as well as B_2 , the aptamer with the antiterminator sequence. The kinetic model described mathematically in the Supporting Material can be used to extract parameters that most closely fit the measured dependence on $[M]$ for the FMN riboswitch (9). When the aptamer sequence is transcribed, the transcript favors the aptamer folded state, and when the antiterminator sequence is transcribed, the folding pattern changes in favor of forming the antiterminator stem with disruption of the aptamer folded structure (9). Thus, there are restraints on the folding rates, $k_{f1} > k_{-f1}$ and $k_{f2} < k_{-f2}$. We also assume the same association (dissociation) rate constant for metabolite binding to B^* , B_2^* , and B_{2t}^* because there is little change in the results when the values of

k_{b2} and k_{b3} are drastically altered. In addition, because we only allow the folded states of the aptamer to bind M the effective K_D is a convolution of the folding rates and the binding rate. Thus, even though k_b is the same the decrease in the folding rate as the transcript length increases effectively decreases K_D . The values of the transitions rates that reproduce the measured f_{ter} (blue squares in Fig. 2) are listed in Table 1. The folding rates k_{f1} and k_{f2} are within an order of magnitude of the theoretical prediction based on, $k_f \sim k_0 e^{-\sqrt{N}}$, $k_0 \sim 10^6 \text{ s}^{-1}$, where N is the number of nucleotides (14,15). Moreover, the rate k_{f1} we obtained is in the same order of magnitude of the folding rate of other riboswitch aptamer with similar lengths observed in experiments (16). Thus, for the purposes of quantitatively describing the in vitro experiments we need only two kinetic rates (k_{-f1} and k_{-f2}).

The folding rate of the aptamer is comparable to k_{f1} (Fig. 1). The transition rate (k_{-f2}) from B_2^* (Fig. 1) to B_2 is 2–3 times the rate of transcription elongation to the stage where the terminator sequence is transcribed (k_{f2}). Because the results are not sensitive to k_{-f1} , if the other rates are fixed, we choose $k_{-f1} \sim k_{-f2}$ because both involve unfolding of the folded aptamer structure. With this assumption, the parameter set that emerges when our model is used to quantitatively describe (see Fig. 2) the in vitro kinetic experiments is unique. In addition, under these conditions, the regulation of transcription termination works when $[M]$ is in large excess over RNA transcript, when $[M]_0/[B]_0 > 10$. With $[M] = 1 \mu\text{M}$ for metabolite concentration and $k_b = 0.1 \mu\text{M}^{-1}\text{s}^{-1}$, the binding time is $\sim 10 \text{ s}$, which is of the same order of magnitude as the transcription elongation rate and the folding rate of the antiterminator stem. Consequently, the metabolite binding is unlikely to reach equilibrium before formation of the antiterminator stem. Large excess of metabolite, exceeding the equilibrium K_D

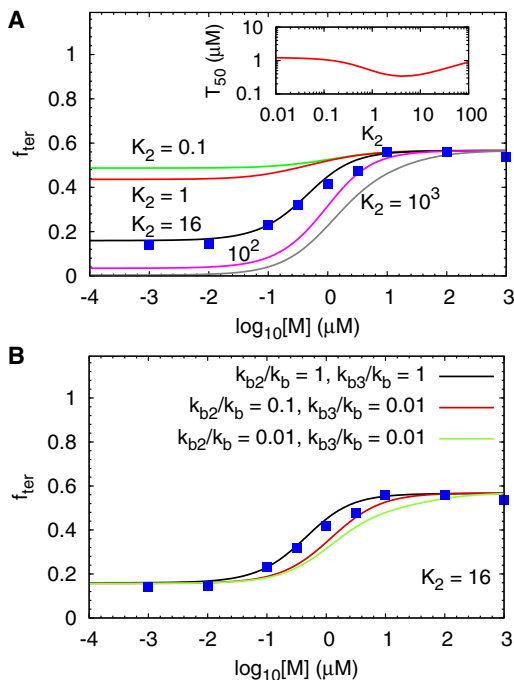


FIGURE 2 Dependence of transcription termination on metabolite concentration without feedback. (A) Fraction of terminated RNA transcripts, f_{ter} , as a function of the logarithm of the metabolite concentration for different values of $K_2 \equiv k_{-f2}/k_{f2}$ with $k_{b2} = k_{b3} = k_b$. Parameters that reproduce the in vitro experimental f_{ter} are listed in Table 1. The inset in (A) shows the half-response metabolite concentration, T_{50} , as a function of K_2 . (B) Sensitivity of f_{ter} to different values of k_{b2} and k_{b3} . Except for modest changes in T_{50} there is little change in f_{ter} when the binding rates are drastically altered. The blue points in (A) and (B) are data from experiments on FMN riboswitch (9).

TABLE 1 Kinetic parameters for model in Fig. 1 without feedback

k_{f1}^*	k_{-f1}	k_{f2}	k_{-f2}	k_{r1}^\dagger	k_{r2}^\dagger	k_b^{\ddagger}	k_{-b}^\dagger
0.1	0.04	2.5×10^{-3}	0.04	0.1	0.016	0.1	10^{-3}

*In unit of s^{-1} for all rates except k_b .

† Values from experimental data (9).

‡ In unit of $\mu\text{M}^{-1}\text{s}^{-1}$.

($\sim 10 \text{ nM}$) for FMN binding to B_2^* , over RNA transcript is needed for the metabolites to bind the riboswitches with sufficient speed to regulate transcription under the conditions explored in experiments (9).

RESULTS

Dependence of f_{ter} on K_2

We investigated how f_{ter} depends on variations in the transition rates around the parameter set listed in Table 1. Fig. 2 shows that the fraction of terminated transcripts converges to the same value in the limit of high metabolite concentration, independent of $K_2 \equiv k_{-f2}/k_{f2}$, while keeping the other parameters fixed. At high $[M]$, B^* and B_2^* are always metabolite bound, which results in very low $[B_2^*]$. Hence, varying k_{-f2} does not affect f_{ter} at high $[M]$. In the limit of low $[M]$, f_{ter} decreases as K_2 increases because k_{-f2} exceeds the effective binding rate $k_b[M]$ so that B_2 is preferentially populated.

The effective metabolite concentration T_{50} , at which

$$\frac{f_{ter}(T_{50}) - f_{ter}^L}{f_{ter}^H - f_{ter}^L} = 0.5, \quad (1)$$

where f_{ter}^H (f_{ter}^L) is the value of f_{ter} at high (low) $[M]$, does not change much as K_2 is varied (see the inset in Fig. 2). Even when K_2 is small $T_{50}/K_D > 1$ implying the concentration of $[M]$ is in excess of the equilibrium K_D to effect binding to B_2^* . Because the population of B_2 is favored as K_2 increases, it follows that f_{ter} decreases at all concentrations of the metabolite as K_2 is changed from a low to a high value (Fig. 2). In addition, the transcription rate from B_2 (or B_2^*) to the next stage where terminator sequence forms (k_{f2}) is about one order of magnitude larger than k_{f2} , which means that at low or normal metabolite concentration, transitions between B_2 and B_2^* states do not reach equilibrium before the terminator sequence is transcribed—a result that also follows from the inequality $T_{50} > K_D$. Finally, the dissociation rate constant is much smaller than k_{f2} , which indicates that once the metabolite is bound, the bound state remains stable through transcription termination. Hence, the riboswitch is in the kinetically driven regime with the parameters used here—a conclusion that was reached in the previous study (9).

Dynamic range and thermodynamic control

Thermodynamic equilibrium between B_2 and B_2^* can be reached only if the transcription speed is much slower

than the transition rates between different folding patterns and the association rate with metabolites (Fig. 1). We varied the transcription speed to probe how the riboswitch can be driven from kinetic to thermodynamic control, which can be experimentally realized by increasing the pausing time, achievable by adding transcription factors, such as NusA. The dependence of f_{ter} on $[M]$ at various $\gamma_2 \equiv k_{t2} / k_{f2}$ values shows that, in the limit of low metabolite concentration, f_{ter} is roughly equal to the fraction of folded aptamer $f_{B_2^*} \approx k_{f2} / (k_{f2} + k_{-f2}) \sim 0.06$. At high metabolite concentrations, almost all riboswitches are metabolite bound, and transcription is terminated with high probability (Fig. 3 A). As γ_2 increases, the system transitions to a kinetically driven regime and the probability that the transcription is terminated at high $[M]$ decreases, whereas the fraction of terminated transcript at low $[M]$ increases.

Interestingly, at high $[M]$ we find that f_{ter} decreases as γ_2 increases because in this limit the folded B_2^* has insufficient time to make a transition to B_2 . As a result the population of B_2 decreases at high γ_2 , resulting in a reduction in f_{ter} (Fig. 3 A). Surprisingly, the exact opposite result is obtained at low $[M]$ as γ_2 is varied. At low $[M]$ and small γ_2 the binding rate $k_b[M]$ is small enough that the transition to B_2 occurs with high probability resulting in a decrease in f_{ter} . As γ_2 increases, the flux from B_2^* to B_2 decreases and the pathway to B_2^* from B^* becomes relevant leading to an increase in f_{ter} at low $[M]$ (Fig. 3 A). Thus, at high γ_2 and low $[M]$ the extent of transcription termination is controlled by $K_1 \equiv k_{-f1} / k_{f1}$ and $\gamma_1 \equiv k_{t1} / k_{f1}$. The value of T_{50} increases substantially relative to K_D as γ_2 increases (see the inset in Fig. 3 A). Even when γ_2 is very small T_{50} exceeds K_D implying that it is difficult to drive the FMN riboswitch to thermodynamic control under the conditions used in experiments (9).

Fig. 3 B shows the dynamic range $\eta \equiv f_{ter}^H - f_{ter}^L$ as a function of K_2 for different values of γ_2 . The riboswitch func-

tions with maximal dynamic range when the system is nearly under thermodynamic control corresponding to small K_2 values. The range of T_{50} is between $0.1 \mu M$ ($\approx 100K_D$) and $1 \mu M$ ($\approx 1000K_D$) for $\gamma_2 > 1$ (Fig. 3 C). When the unfolding rate of the aptamer folded structure (B_2^*) is comparable to the speed of transcription to the terminator sequence, $K_2 \sim \gamma_2$, T_{50} has the smallest value. The minimum T_{50} decreases as γ_2 decreases, and T_{50} becomes less dependent on K_2 when $K_2 < 1$. When $\gamma_2 \ll 1$, as shown in Fig. 3 D, the probability of transcription termination approaches unity in the limit of high metabolite concentration at all values of K_2 . On the other hand, in the limit of low metabolite concentration ($k_b[M]$ is small), f_{ter} increases and T_{50} decreases as K_2 decreases. The results in Fig. 3 show that the efficiency of the riboswitch function is determined by a compromise between the need to maximize η (γ_2 should be small) and the ability to terminate transcription (γ_2 should be large).

Effect of aptamer folding rates on f_{ter}

In the kinetically driven regime ($\gamma_2 > 1$), the probability of transcription termination depends on the fraction of the aptamer formed state before transcription of the antiterminator sequence. This fraction can be changed by altering k_{f1} , or equivalently the ratio $K_1 \equiv k_{-f1} / k_{f1}$, or by varying the transcription speed from the aptamer domain sequence to antiterminator sequence, k_{t1} . When $K_1 \gg 1$, most of the riboswitches do not form stable folded aptamer domain B^* (Fig. 1), resulting in a very small fraction of transcription termination and low response to changes in the metabolite concentration. As the transition rate from the unfolded state (B) to the folded aptamer state (B^*) increases relative to the reverse transition rate, the fraction of terminated transcripts and dynamic range increases (Fig. 4 A). In the limit of high

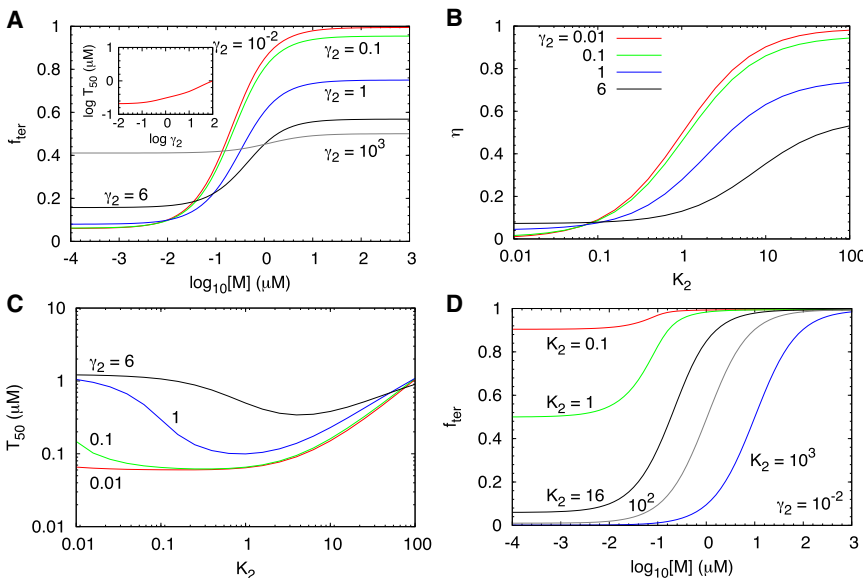


FIGURE 3 Speed of transcription and gene expression. (A) Fraction of terminated RNA transcripts, f_{ter} , as a function of the logarithm of metabolite concentration for different values of $\gamma_2 \equiv k_{t2} / k_{f2}$. The parameters that reproduce the experimental f_{ter} results in $\gamma_2 = 6$. The inset shows $\log(T_{50})$ as a function of $\log(\gamma_2)$. (B) The dynamic range $\eta \equiv f_{ter}^H - f_{ter}^L$, where f_{ter}^H (f_{ter}^L) is the value of f_{ter} at high (low) metabolite concentration, as a function of K_2 . (C) Variation of T_{50} as a function of K_2 . (D) Fraction of terminated RNA transcripts as a function of the logarithm of metabolite concentration for different values of K_2 with $\gamma_2 = 10^{-2}$. Other parameters used are listed in Table 1.

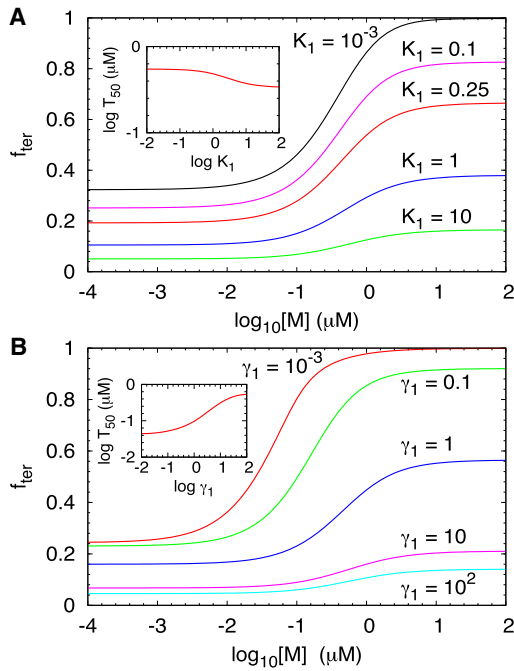


FIGURE 4 Aptamer folding rates and f_{ter} . (A) Fraction of terminated RNA transcripts as a function of $\log([M])$ for different values of $K_1 \equiv k_{-f1}/k_{f1}$ using the parameters listed in Table 1 except for k_{-f1} . (B) Fraction of terminated RNA transcripts as a function of $\log([M])$ for different values of $\gamma_1 \equiv k_{t1}/k_{f1}$. Inset shows the dependence of T_{50} on γ_1 .

$[M]$, the probability of transcription termination approaches 1 when $K_1 \ll 1$, whereas in the low $[M]$ limit, almost all the riboswitches are aptamer folded but without metabolite bound (B^*) before transcription to antiterminator sequence. Just as in Fig. 2, T_{50} is not sensitive to changes in K_1 (see inset in Fig. 4 A).

Fig. 4 B shows the concentration dependence of the fraction of terminated transcripts for different transcription rates to the antiterminator sequence, or the ratio $\gamma_1 \equiv k_{t1}/k_{f1}$. When the transcription rate is much faster than the folding rate, the riboswitch does not have enough time to form the aptamer folded structure, which results in a low fraction of terminated transcripts and low response to metabolite concentration change. When the transcription rate is much slower than the folding rate, the folded and unfolded states of the aptamer are able to reach equilibrium before transcription to antiterminator sequence. In the high metabolite concentration limit, the riboswitch is always metabolite bound resulting in transcription termination. At low $[M]$, the riboswitch does not bind the metabolite. The fraction of aptamer formed state without bound metabolite is $k_{f1}/(k_{f1} + k_{-f1}) \approx f_{ter}$ before transcription to the antiterminator sequence. There is substantial variation in T_{50} as γ_1 changes as the inset in Fig. 4 B shows. Thus, besides the speed of transcription and the binding rates, the folding rates of the aptamers have considerable influence on f_{ter} (compare insets in Fig. 3 A and Fig. 4 B).

Transcription with negative feedback loop

Most riboswitches regulate gene expression of the downstream platform that encodes for proteins involved in the production of the specific metabolite that itself binds to the riboswitch (Fig. 1). Therefore, sensing and binding of its own metabolite by the riboswitch acts as a feedback to control gene expression. For riboswitches that suppress gene expression by binding to metabolites with high selectivity (for example, guanine riboswitches or FMN riboswitches) such feedback loop is an example of negative autoregulation, which has been widely studied in gene regulation networks associated with transcription factors (17). We include the role negative feedback plays in regulating transcription termination by generalizing the in vitro kinetic model considered in the previous section. Our minimal model, illustrated in Fig. 1 and described in detail in the Supporting Material, provides a framework for interpreting future in vivo experiments.

We consider transcription and translation in a cell and take into account RNA degradation and cell expansion. The transcription process is similar to that described without a feedback loop, except now we include the effect of cell expansion and RNA degradation. We assume that the cell grows at a rate of $\mu = 5 \times 10^{-4} \text{ s}^{-1}$, resulting in a typical doubling time of $\ln 2/\mu \sim 20$ minutes for an *Escherichia coli* cell, and that the degradation rate of the fully transcribed RNA or terminated RNA transcript is k_{d1} . The values of k_{d1} , and other parameters in the feedback loop are in Table 2. The fully transcribed RNA serves as a template for the translation of the protein (P) that synthesizes metabolite M_0 , which is then converted to an active form M by the enzyme E encoded by the gene O_F (Fig. 1). The species M , with a degradation rate of k_{d3} , is the target metabolite that binds to the riboswitch.

In the case of FMN riboswitches, M_0 represents riboflavin, the eventual product encoded by the gene *ribD* (O_R), which is subsequently converted to FMN by flavokinase (E), synthesized by the gene *ribC* (O_F). The degradation rate k_{d3} takes into account the effect of conversion from FMN to FAD (flavin adenine dinucleotide) by FAD synthetase in vivo (see the Supporting Material for more details). However, we neglect the potential binding of FAD to the riboswitch because there is a 60-fold difference

TABLE 2 Additional kinetic parameters for model in Fig. 1 with negative feedback

k_{t3}^*	K_1	k_2^\dagger	k_3^\ddagger	k_{d1}^\S	k_{d2}^\P	k_{d3}^{\parallel}	μ
0.01	0.016	0.3	0.064	2.3×10^{-3}	2.7×10^{-4}	4.5×10^{-3}	5×10^{-4}

*In unit of s^{-1} for all rates.

[†]Ref. (26).

[‡]Ref. (27).

[§]Ref. (28).

[¶]Ref. (29).

^{||}See the Supporting Material.

(or potentially even larger factor in the absence of FMN) in the binding of FMN and FAD to the FMN riboswitch (18). In the model with negative feedback the extent of regulation by riboswitches is expressed in terms of the production of the protein P (Fig. 1).

We assume that the activated level of the operon, O_R , for transcription initiation of the riboswitch is a constant, and set $[DNA] = [O_R] = 2.5$ nM, which is equivalent to one DNA molecule in an *E. coli* cell, and assume that the aptamer sequence, B , is produced with an effective rate constant $k_1 = 0.016$ s⁻¹, taking into account the transcription initiation rate (~ 50 s between initiation events (19,20)) and the typical transcription speed, $\sim 10 - 35$ nucleotides/s (21). With these parameters fixed, which are used for illustrative purposes only, we can study the effect of feedback by varying the effective rate k_F , at which E is produced from O_F . We set $[O_F] = [O_R]$. If E is produced at a rate similar to that of protein P , without feedback, then $k_F \sim 1$ s⁻¹, which we set as a reference rate k_{F0} (see the Supporting Material for details). At this rate, the steady-state level of enzyme E is $\sim 10^3$ copies per cell. The variation of rate k_F can result from delays or speed up in the process of the transcription from O_F or translation of E , or even deficiency in O_F .

Dependence of $[P]$ on enzyme production and metabolite binding rates

We assess the extent of regulation due to feedback by the changes in the protein level expression, $[P]$, as the parameters in the network are varied. The results in Fig. 5 A show that when k_F / k_{F0} is low, very few active metabolites are formed to suppress protein expression. Consequently, the expression level of protein does not change at low k_F / k_{F0} at all values of γ_2 (Fig. 5 A). This finding explains the observation that deficiency in *ribC* (O_F in Fig. 1), the gene that encodes for flavokinase (E in Fig. 1), causes accumulation of riboflavin (M_0 in Fig. 1) without converting it to FMN, and thus cannot suppress the synthesis of riboflavin (22,23). When k_F increases to about $10^{-3}k_{F0}$, the expression of the protein starts to be suppressed. There is a substantial suppression of protein concentration (Fig. 5 A) at all γ_2 values when $k_F / k_{F0} > 10^{-2}$. As k_F exceeds $0.1 k_{F0}$, the suppression begins to saturate (Fig. 5 A) because most of M_0 produced are converted to M , and the $[P]$ level is essentially determined by the production of $[M]_0$, which is independent of k_F . Thus, at all γ_2 values, $[P]$ level varies between two steady-state values as k_F is changed.

In contrast to the results in Fig. 5 A, the extent of regulation ($[P]$ levels) varies greatly with the binding rate constant of metabolites while keeping K_D fixed at 10 nM (Fig. 5 B). Changes in $[P]$ as k_b is varied, which affect synthesis of M_0 (Fig. 1), depend on k_F / k_{F0} . When $k_F \geq k_{F0}$, most of the aptamer folded structures are metabolite bound at the experi-

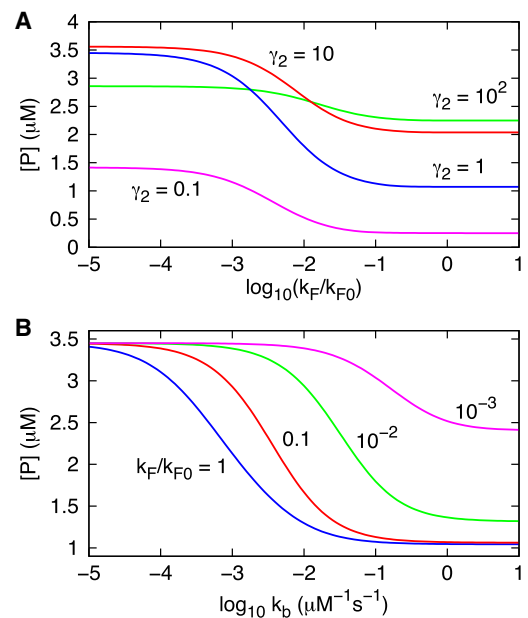


FIGURE 5 Effect of negative feedback. (A) Protein (P in Fig. 1) concentration at different γ_2 values as a function of the logarithm of k_F , the production rate constant of enzyme E that produces the metabolite M , relative to $k_{F0} = 1$ s⁻¹. The parameters are given in Table 1 and Table 2 except k_{i2} . (B) The extent of regulation expressed in terms of protein level as a function of the logarithm of association rate constant k_b for metabolite binding. The parameters are listed in Table 1 and Table 2 except k_b and k_{-b} . K_D is fixed at 10 nM.

mental value of $k_b = 0.1 \mu\text{M}^{-1}\text{s}^{-1}$, and hence the level of protein expression is suppressed. Therefore, with $\sim 10^3$ copies of enzyme E in a cell, the production of $[P]$ decreases substantially even if the binding rate constant is small. Binding occurs because the concentration of active metabolites ($\sim 25 \mu\text{M}$) is far larger than RNA transcripts (~ 10 nM), resulting in a high effective binding rate $k_b[M]$. The ability to suppress protein production decreases if the binding rate constant is smaller than the experimental value by more than one order of magnitude, or when the value of k_F decreases. Not surprisingly, when k_F is very low, the dependence of binding rate on expression of P decreases. As a consequence the changes in P production decrease greatly as k_F / k_{F0} decreases (Fig. 5 B). Thus, only over a small range of k_b and k_F / k_{F0} does the riboswitch function with sufficient dynamic range.

Interplay between cotranscriptional folding and transcription speed

The dependence of transcription rate on the extent of regulation, shown in Fig. 6, exhibits three distinct functional modality depending on the value of k_{i2} relative to k_{-i2} . First, consider the case with $k_F = 0$ (black line in Fig. 6 A). If $k_{i2} \gg k_{-i2}$, the fraction of fully transcribed RNA (Fig. 6 A), $f_{tra} = 1 - f_{ter}$, becomes

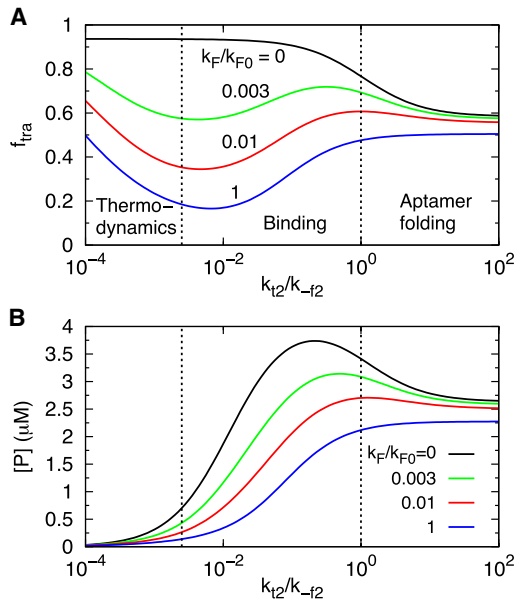


FIGURE 6 Role of k_{12} on negative feedback. (A) The fraction of fully transcribed RNA, $f_{tra} = 1 - f_{ter}$, as a function of k_{12}/k_{-f2} . The numbers give values of k_F/k_{F0} with $k_{F0} = 1 \text{ s}^{-1}$. The dependence of f_{tra} on k_{12}/k_{-f2} shows three regimes: thermodynamic controlled regime for low k_{12} ($k_{12}/k_{-f2} < 0.025$, or $k_{12} < 0.1k_{-b}$), aptamer folding dominated regime for high k_{12} ($k_{12} > k_{-f2}$), and intermediate regime with significant metabolite binding. (B) The P concentration as a function of k_{12}/k_{-f2} at different k_F/k_{F0} values (as described in (A)).

$$f_{tra} \equiv \frac{[RNA]}{[RNA]_0} \approx \frac{K_1 \left(1 + \frac{k_{t1} + \mu}{k_{-f1}}\right)}{1 + K_1 \left(1 + \frac{k_{t1} + \mu}{k_{-f1}}\right)}, \quad (2)$$

where $[RNA]_0$ is the sum of concentration of the fully transcribed and terminated RNA transcripts, and $K_1 \equiv k_{-f1}/k_{f1}$. In this limit, f_{tra} depends predominantly on the folding transition rate before the antiterminator sequence (B_2) is transcribed (Fig. 1). Hence, f_{tra} is a function of k_{t1} , k_{-f1} , and the rate of cell expansion. When k_{12}/k_{-f2} decreases, co-transcriptional folding results in the formation of the antiterminator stem, which prevents transcription termination. If $k_{12} \ll k_{-f2}$ and $\mu \ll k_{-f2}$, then

$$f_{tra} \approx \frac{K_2}{K_2 + 1} = \frac{k_{-f2}}{k_{f2} + k_{-f2}}, \quad (3)$$

where $K_2 \equiv k_{-f2}/k_{f2}$. In this limit, B_2 and B_2^* (Fig. 1) are in equilibrium. These results are the same as those in the limit of low metabolite concentration without the feedback loop (Fig. 3 A).

For finite k_F , when k_{12} is fast relative to k_{-f2} the expression level of protein P is nearly independent of k_{12} (Fig. 6 B). In this regime transcription termination and hence the extent of completed transcription is determined by the folding rates of the aptamer, which is not greatly affected

by negative feedback. When the transcription speed decreases, the expression of protein P increases for small k_F (Fig. 6 B). The expression level of P reaches a peak when $k_{12}/k_{-f2} \sim 0.1 - 1$, and it disappears when $k_F/k_{F0} \geq 1$ because the metabolite binding becomes significant enough to stabilize the folded aptamer structure and offset the effect of formation of the antiterminator stem. This is illustrated in Fig. 6 A, which shows that f_{tra} decreases significantly when k_{12} goes below $0.1k_{-f2}$ and reaches a minimum at $k_{12}/k_{-f2} \sim 0.01$. The dependence of $[P]$ on k_{12}/k_{-f2} is maximal when $k_{12}/k_{-f2} \sim 0.01 - 0.1$. When the transcription rate decreases further ($k_{12} \leq 0.1k_{-b}$, or $k_{12}/k_{-f2} \leq 2.5 \times 10^{-3}$ as shown by the left dashed line in Fig. 6 A), the fraction of fully transcribed RNA increases sharply because the transcription rate is slow enough for the dissociation of metabolites from riboswitches to occur significantly. The system can establish thermodynamic equilibrium, which increases the favorability of the formation of antiterminator stem when k_{12} decreases resulting in decreasing effective binding rate $k_b[M]$. However, the overall expression level of protein P becomes very low because slow transcription results in a decrease in P production. In addition, there is also significant probability of RNA degradation, which also results in a decrease in P expression. Therefore, the extent of regulation due to the negative feedback of metabolite binding has a maximal effect when $k_{12}/k_{-f2} \sim 0.01$ where the protein expression is suppressed by metabolite binding by as large as 85%.

Dynamic phase diagram: competition between folding, transcription, and binding rates

To have a more complete picture on how the interplay between folding of RNA transcripts, transcription, and metabolite binding regulate the expression of P , we study the dependence of $[P]$ on the transcription rates and the effective binding rate $k_b[M]$. The dynamic phase diagram in Fig. 7 is calculated by varying both k_{t1} , (k_{12}), and k_b with $K_D = 10 \text{ nM}$. In the first stage of transcription elongation, i.e., after the aptamer sequence is transcribed, the formation of the aptamer structure is the key step in regulating transcription termination. Thus, the folding rate k_{f1} and the effective metabolite binding rate are the key rates in competition with k_{t1} for regulation of $[P]$. Fig. 7 A shows three regimes for the dependence of $[P]$ on k_{t1} and $k_b[M]$. In regime I, $k_{t1} > k_{f1}$, the folding rate is slow relative to transcription to the next stage (Fig. 1). Thus, the aptamer structure does not have enough time to form. The dominant flux is from B to B_2 , which leads to high probability of fully transcribed RNA downstream because of the low transition rate from B_2 to B_2^* . The metabolite binding has little effect on protein expression in this regime, particularly for large k_{t1}/k_{f1} , and hence the protein is highly expressed. In regime II, $k_b[M] < k_{t1} < k_{f1}$, the aptamer has enough time to fold but the metabolite binding is slow.

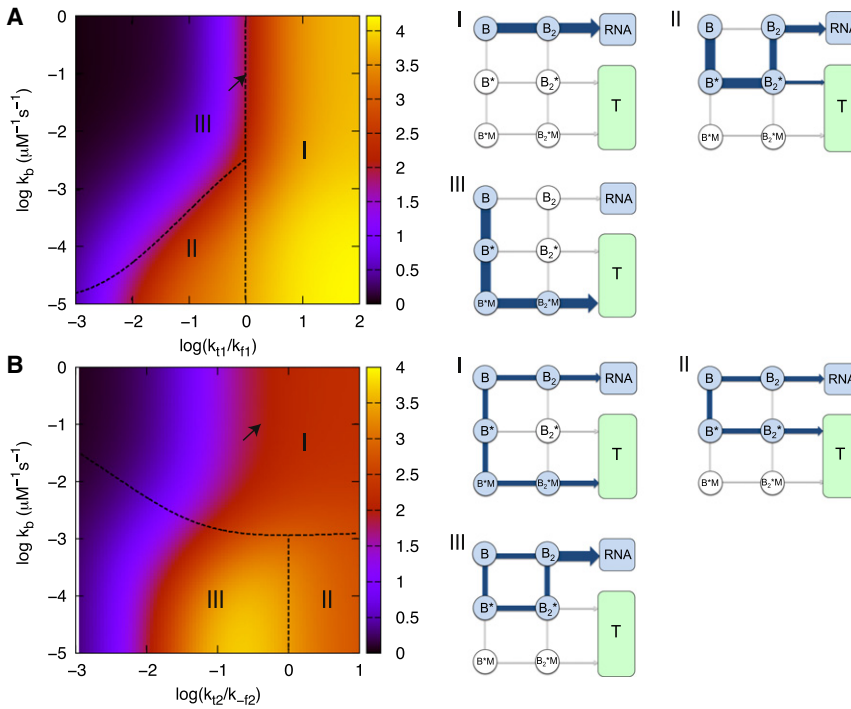


FIGURE 7 Dependence of protein production on the network parameters with feedback. (A) Protein levels as functions of k_{t1}/k_{f1} and k_b with negative feedback using parameters in Table 1 and Table 2. The scale for the $[P]$ production is shown in the color spectrum. The dependence of $[P]$ on k_{t1} and k_b is categorized into three regimes separating regime II and regime III satisfy $k_b[M] = k_{t1}$. The major pathway in the transcription process in each regime is shown on the right. The arrow indicates the data point resulting from using the value of k_{t1} and k_b in Table 1. (B) Expression level of proteins as functions of k_{t2}/k_{-f2} and k_b with negative feedback using the parameters in Table 1 and Table 2. The dependence of $[P]$ on k_{t2} and $k_b[M]$ is categorized into three regimes. Points on the dashed line separating regime I and regime II/III satisfy $k_b[M] = k_{-f2}$. The corresponding major transcription pathways are shown on the right. The data point corresponding to the arrow results from using the value of k_{t2} and k_b in Table 1.

The dominant flux is $B \rightarrow B^* \rightarrow B_2^*$, leading to formation of antitermination stem ($B_2^* \rightarrow B_2$) or transcription termination ($B_2^* \rightarrow B_{2t}^*$). The expression level of protein is thus mainly determined by k_{-f2} and k_{t2} , and the protein production is partially suppressed in this regime. In regime III, $k_{t1} < k_{f1}$ and $k_{t1} < k_b[M]$, the aptamer has sufficient time to both fold and bind metabolite, the dominant pathway is $B \rightarrow B^* \rightarrow B^*M \rightarrow B_2^*M$, leading to transcription termination. The protein production is highly suppressed in this regime. The results using parameters from Table 1 and Table 2 ($k_{t1} = k_{f1}$ and $k_b[M]/k_{f1} \sim 25$) fall on the interface of regime I and regime III, as shown by the arrow in Fig. 7 A. The metabolite binding does not reach thermodynamic equilibrium due to a low dissociation constant. However, the effective binding rate is high because the steady-state concentration of metabolites ($\sim 25 \mu\text{M}$) is in large excess over RNA transcripts. Thus, the riboswitch is kinetically driven under this condition even when feedback is included.

With k_{t1} comparable to k_{f1} , at the second stage of transcription elongation the key step against transcription termination is the formation of the antiterminator stem ($B_2^* \rightarrow B_2$). Fig. 7 B also shows three regimes for the dependence of $[P]$ on k_{t2} and $k_b[M]$ relative to k_{-f2} , and the associated most probable pathways are displayed on the right. In regime I, $k_b[M] > k_{-f2}$, the effective binding rate competes favorably with $B_2^* \rightarrow B_2$ transition so that B_2 , if populated, is not likely to form the antiterminator stem. However, in this regime, the effective binding rate is also likely to be larger than k_{t1} , resulting in most of the metabolite binding occurring at the first stage of transcription. Protein production is partially

suppressed with the flux toward transcription termination flowing through $B^*M \rightarrow B_2^*M \rightarrow T$ (terminated transcript). In regime II, $k_b[M] < k_{-f2} < k_{t2}$, both the metabolite binding and $B_2^* \rightarrow B_2$ transition are too slow to occur. The protein production level is mainly determined by k_{t1} and k_{f1} . The major pathways are $B \rightarrow B_2 \rightarrow \text{RNA}$ and $B \rightarrow B^* \rightarrow B_2^* \rightarrow T$, leading to partial protein suppression. In regime III, $k_b[M] < k_{-f2}$ and $k_{t2} < k_{-f2}$, metabolite binding is too slow to occur, but the riboswitch has enough time to form the antiterminator stem before the terminator sequence is transcribed. The major flux from B_2^* flows to B_2 , leading to fully transcribed RNA, and proteins are highly expressed. We note that using the parameters from Table 1 and Table 2 ($k_{t2}/k_{-f2} = 0.4$ and $k_bM/k_{-f2} \sim 60$), the result falls in regime I with partial protein suppression. Among the three regimes, regime I has efficient negative feedback, whereas the slow metabolite binding in regime II and regime III make results resemble those without feedback. The dynamic phase diagrams predict results with limiting cases of various parameters, whose values may be within range in vivo and most certainly in vitro.

Role of feedback in response to DNA bursts

To assess how feedback affects the response to a sudden burst in DNA concentration we calculated the time dependent changes in the protein concentration,

$$\frac{\Delta P(t)}{\Delta P_{st}} = \frac{P_{[DNA]_f}(t) - P_{[DNA]_i}(t)}{P_{[DNA]_f}^{st} - P_{[DNA]_i}^{st}}, \quad (4)$$

when the DNA concentration is switched from $[DNA]_i$ to $[DNA]_f$. In Eq. 4 st stands for steady state. Fig. 8 A shows the response time, defined as the time needed to reach halfway to the new steady-state level (dashed line in Fig. 8 A), for $[DNA]_f = 3.75$ nM and $[DNA]_i = 2.5$ nM using folding and unfolding rates one order of magnitude larger than those in Table 1. Small transient fluctuations in DNA concentration could arise from environmental stresses, and hence it is interesting to examine the response of the network to such changes. The values of the folding rates from Table 1 result in little difference in response time between cases with negative feedback and without feedback. However, with larger folding rates, the response time for the systems with negative feedback is significantly shorter than without feedback (Fig. 8 A). The fractional change of the fully transcribed RNA, $\Delta F(t) \equiv f_{tra}([DNA]_f, t) - f_{tra}([DNA]_i, t)$ (Fig. 8 B), shows a slight increase with overshoot initially before settling into a steady-state level lower than the original one in the case of negative feedback (blue line in Fig. 8 B). For the case without feedback, the fraction of fully transcribed RNA decreases initially before reaching the expected steady-state level (red line in Fig. 8 B).

With negative feedback and 10-fold increase in overall folding and unfolding rates, the fractional increase in the protein steady-state level, $\delta P_{st} \equiv (P_{[DNA]_f}^{st} - P_{[DNA]_i}^{st})/P_{[DNA]_i}^{st}$, in response to the increase in DNA level, $\delta D = ([DNA]_f - [DNA]_i)/[DNA]_i$, is reduced by more than half of that in the case without feedback for a certain range of parameters, as shown in Fig. 8, C and D. Without feedback, $\delta P_{st} = \delta D$. Negative feedback noticeably reduces the variations of expression in protein due to DNA level change. Substantial

reduction occurs when the effective binding rate is comparable to k_{-f2} and when $k_{t2} \leq k_{-f2}$ (the interface between regime I and regime III in Fig. 8 D).

DISCUSSION

Transcription, regulated by metabolite binding to riboswitches, depends on interplay of a number of timescales that are intrinsic to the cotranscriptional folding of the riboswitch as well as those determined by cellular conditions. For a riboswitch to function with a large dynamic range, transcription levels should change significantly as the metabolite concentration increases from a low to high value. In the high concentration limit, RNA transcript in the aptamer folded state binds a metabolite. Low dissociation rate constant results in the formation of a terminator stem, which subsequently terminates transcription. In the low concentration limit, the aptamer folded state is mostly unbound and can remain folded until transcription termination or can fold to the antiterminator state leading to the transcription of the full RNA. The levels of transcription termination are thus controlled by the transition rates between the aptamer folded and unfolded states.

For in vitro description the efficiency of riboswitch is determined by two conflicting requirements. If η , the dynamic range, is to be maximized, then γ_2 has to be sufficiently low. However, at low γ_2 and realistic values of the metabolite concentration, $f_{ter} \approx 1$, implies the switching function (needed to abort transcription) cannot be achieved. Thus, γ_2 has to have an optimal range ($\gamma_2 \sim (1 - 10)$) for the riboswitch to have sufficient dynamic

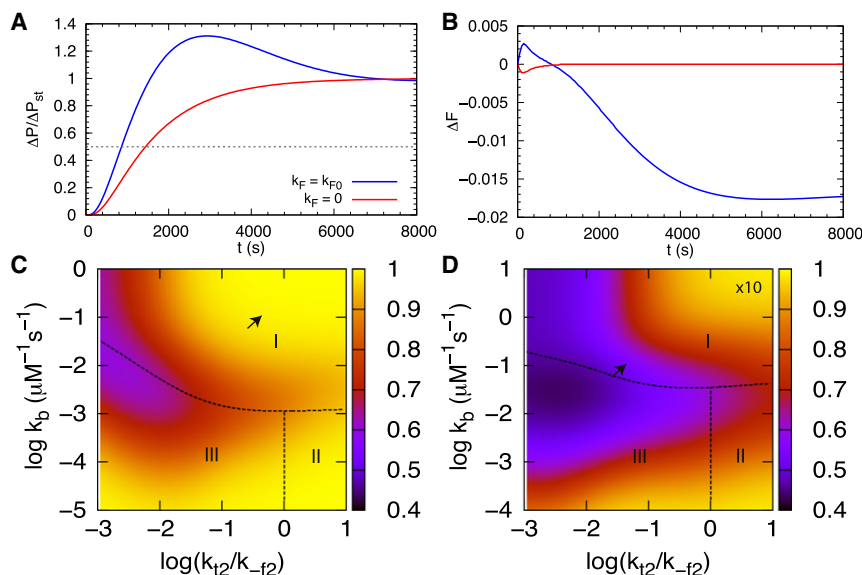


FIGURE 8 Role of feedback to a spike in the DNA concentration. (A) Response of protein level (ΔP) relative to the change of steady-state level (ΔP_{st}) when the DNA level increases by 50%. The response time is 850 s with negative feedback (blue line) and 1450 s without feedback (red line). The values of folding and unfolding rates used are 10-fold larger than those given in Table 1. (B) Response of the fraction of fully transcribed RNA, ΔF , when the DNA level increases by 50%. The fraction of fully transcribed RNA increases initially with negative feedback (blue line) and decreases initially without feedback (red line) before settling to a new steady state. (C) Fractional change in protein steady-state level relative to that in DNA concentration, $\delta P_{st}/\delta D$, in response to a 50% rise in DNA level, as a function of k_{t2}/k_{-f2} and k_b for the riboswitch network with negative feedback using parameters in Table 1. Points on the dashed line separating regime I and regime II/III satisfy $k_b[M] = k_{-f2}$. (D) Same as (C) with the overall folding and unfolding rates being 10-fold greater than those in Table 1. The arrow indicates the data point when k_{t2} and k_b are at the values from Table 1.

range without compromising the ability to switch from an on to off state.

In the presence of a negative feedback loop the concentration of target metabolites is also regulated by gene expression. Under nominal operating conditions ($k_{12}/k_{-f2} \sim 0.01 - 0.1$) binding of target metabolites, products of the downstream gene that riboswitches regulate, significantly suppresses the expression of proteins. Negative feedback suppresses the protein level by about half relative to the case without feedback. In vivo, the presence of RNA binding proteins, such as NusA, may increase the pausing times, thus effectively reducing the transcription rates. Thus, the repression of the protein level by the riboswitch through metabolite binding may be up to 10-fold. Faster RNA folding and unfolding rates than those we obtained may also increase the suppression by negative feedback and broaden the range of transcription rates over which maximal suppression occurs. These predictions are amenable to experimental test.

In response to changes in the active operon level, the negative feedback speeds up the response time of expression and modestly reduces the percentage change in the protein level relative to change in the operon level. The steady-state level of expression for autoregulation varies as a square root of the DNA concentration. Adaptive biological systems may minimize the variation in gene expression to keep the systems functioning normally even when the environments change drastically. One may need to consider more complex networks than the single autoregulation in the transcription network to find near perfect adaptation to the environmental change (24).

Riboswitches provide novel ways to engineer biological circuits to control gene expression by binding small molecules. As found in tandem riboswitches (6,7), multiple riboswitches can be engineered to control a single gene with greater regulatory complexity or increase in the dynamic range of gene control. Synthetic riboswitches have been successfully used to control the chemotaxis of bacteria (25). Our study provides a physical basis for not only analyzing future experiments but also in anticipating their outcomes.

SUPPORTING MATERIAL

Kinetic model and steady state solutions are available at [http://www.biophysj.org/biophysj/supplemental/S0006-3495\(12\)01131-9](http://www.biophysj.org/biophysj/supplemental/S0006-3495(12)01131-9).

We thank Michael Hinczewski for constructive suggestions and advice.

This work was supported in part by a grant from the National Science Foundation through grant No. CHE09-10433.

REFERENCES

- Cheah, M. T., A. Wachter, ..., R. R. Breaker. 2007. Control of alternative RNA splicing and gene expression by eukaryotic riboswitches. *Nature*. 447:497–500.
- Montange, R. K., and R. T. Batey. 2008. Riboswitches: emerging themes in RNA structure and function. *Annu. Rev. Biophys.* 37: 117–133.
- Winkler, W. C., and R. R. Breaker. 2005. Regulation of bacterial gene expression by riboswitches. *Annu. Rev. Microbiol.* 59:487–517.
- Batey, R. T., S. D. Gilbert, and R. K. Montange. 2004. Structure of a natural guanine-responsive riboswitch complexed with the metabolite hypoxanthine. *Nature*. 432:411–415.
- Serganov, A., Y. R. Yuan, ..., D. J. Patel. 2004. Structural basis for discriminative regulation of gene expression by adenine- and guanine-sensing mRNAs. *Chem. Biol.* 11:1729–1741.
- Breaker, R. R. 2008. Complex riboswitches. *Science*. 319:1795–1797.
- Sudarsan, N., M. C. Hammond, ..., R. R. Breaker. 2006. Tandem riboswitch architectures exhibit complex gene control functions. *Science*. 314:300–304.
- Watson, P. Y., and M. J. Fedor. 2011. The glmS riboswitch integrates signals from activating and inhibitory metabolites in vivo. *Nat. Struct. Mol. Biol.* 18:359–363.
- Wickiser, J. K., W. C. Winkler, ..., D. M. Crothers. 2005. The speed of RNA transcription and metabolite binding kinetics operate an FMN riboswitch. *Mol. Cell*. 18:49–60.
- Carothers, J. M., J. A. Goler, ..., J. D. Keasling. 2011. Model-driven engineering of RNA devices to quantitatively program gene expression. *Science*. 334:1716–1719.
- Link, K. H., and R. R. Breaker. 2009. Engineering ligand-responsive gene-control elements: lessons learned from natural riboswitches. *Gene Ther.* 16:1189–1201.
- Beisel, C. L., and C. D. Smolke. 2009. Design principles for riboswitch function. *PLoS Comput. Biol.* 5:e1000363.
- Chen, X., and A. D. Ellington. 2009. Design principles for ligand-sensing, conformation-switching ribozymes. *PLoS Comput. Biol.* 5:e1000620.
- Hyeon, C., and D. Thirumalai. 2012. Chain length determines the folding rates of RNA. *Biophys. J.* 102:L11–L13.
- Thirumalai, D. 1995. From minimal models to real proteins: time scales for protein folding kinetics. *J. Phys. I.* 5:1457–1467.
- Perdrizet, 2nd, G. A., I. Artsimovitch, ..., T. Pan. 2012. Transcriptional pausing coordinates folding of the aptamer domain and the expression platform of a riboswitch. *Proc. Natl. Acad. Sci. USA.* 109:3323–3328.
- Alon, U. 2007. Network motifs: theory and experimental approaches. *Nat. Rev. Genet.* 8:450–461.
- Winkler, W. C., S. Cohen-Chalamish, and R. R. Breaker. 2002. An mRNA structure that controls gene expression by binding FMN. *Proc. Natl. Acad. Sci. USA.* 99:15908–15913.
- Iyer, V., and K. Struhl. 1996. Absolute mRNA levels and transcriptional initiation rates in *Saccharomyces cerevisiae*. *Proc. Natl. Acad. Sci. USA.* 93:5208–5212.
- Larson, D. R., D. Zenklusen, ..., R. H. Singer. 2011. Real-time observation of transcription initiation and elongation on an endogenous yeast gene. *Science*. 332:475–478.
- Uptain, S. M., C. M. Kane, and M. J. Chamberlin. 1997. Basic mechanisms of transcript elongation and its regulation. *Annu. Rev. Biochem.* 66:117–172.
- Gusarov, I. I., R. A. Kreneva, ..., D. A. Perumov. 1997. Primary structure and functional activity of the *Bacillus subtilis* ribC gene. *Mol. Biol. (Mosk.)*. 31:820–825.
- Mack, M. A., A. P. van Loon, and H. P. Hohmann. 1998. Regulation of riboflavin biosynthesis in *Bacillus subtilis* is affected by the activity of the flavokinase/flavin adenine dinucleotide synthetase encoded by ribC. *J. Bacteriol.* 180:950–955.
- Ma, W., A. Trusina, ..., C. Tang. 2009. Defining network topologies that can achieve biochemical adaptation. *Cell*. 138:760–773.

25. Topp, S., and J. P. Gallivan. 2007. Guiding bacteria with small molecules and RNA. *J. Am. Chem. Soc.* 129:6807–6811.
26. McAdams, H. H., and A. Arkin. 1997. Stochastic mechanisms in gene expression. *Proc. Natl. Acad. Sci. USA.* 94:814–819.
27. Schramek, N., A. Bracher, and A. Bacher. 2001. Biosynthesis of riboflavin. Single turnover kinetic analysis of GTP cyclohydrolase II. *J. Biol. Chem.* 276:44157–44162.
28. Bernstein, J. A., A. B. Khodursky, ..., S. N. Cohen. 2002. Global analysis of mRNA decay and abundance in *Escherichia coli* at single-gene resolution using two-color fluorescent DNA microarrays. *Proc. Natl. Acad. Sci. USA.* 99:9697–9702.
29. Belle, A., A. Tanay, ..., E. K. O'Shea. 2006. Quantification of protein half-lives in the budding yeast proteome. *Proc. Natl. Acad. Sci. USA.* 103:13004–13009.